Heat transfer augmentation in concentric elliptic annular by ethylene glycol based nanofluids

CrossMark

H.K. Dawood [a,b], H.A. Mohammed [c,*], Nor Azwadi Che Sidik [d], K.M. Munisamy [a], Omer A. Alawi [d]

[a] Department of Mechanical Engineering, College of Engineering, Universiti Tenaga Nasional, Jalan IKRAM-UNITEN, 43009 Kajang, Selangor, Malaysia
[b] Department of Mechanical Engineering, College of Engineering, University of Anbar, Ramadi, Anbar, Iraq
[c] Department of Energy Engineering, Technical College of Engineering, Duhok Polytechnic University (DPU), 61 Zakho Road- 1006 Mazi Qr, Duhok-Kurdistan Region, Iraq
[d] Department of Thermofluids, Faculty of Mechanical Engineering, Universiti Teknologi Malaysia, 81310 UTM Skudai, Johor Bahru, Malaysia

A R T I C L E   I N F O

A B S T R A C T

In this article, laminar mixed convective heat transfer at different nanofluids flow in an elliptic annulus with constant heat flux boundary condition has been numerically investigated. The three dimensional governing equations (continuity, momentum and energy) are solved using the finite volume method (FVM). The investigation covers Reynolds number and nanoparticle volume fraction in the ranges of 200–1000 and 0–4% respectively. In the present work, four different types of nanofluids are examined in which Al_2O_3, CuO, SiO_2 and ZnO are suspended in the base fluid of ethylene glycol (EG) with different nanoparticle sizes 20, 40, 60 and 80 nm. The results show that SiO_2-EG nanofluid has the highest Nusselt number, followed by Al_2O_3-EG, ZnO-EG, CuO-EG, and lastly pure ethylene glycol. The Nusselt number increased as the nanoparticle volume fraction and Reynolds number increased; however, it decreased as the nanoparticle diameter increased. It is found that the glycerine-SiO_2 shows the best heat transfer enhancement compared with other tested base fluids. Comparisons of the present results with those available in the literature are presented and discussed.

© 2017 Elsevier Ltd. All rights reserved.

1. Introduction

Nowadays after a century of struggling for enhancing industrial heat transfer by fluid mechanics, the low thermal conductivity of conventional fluids such as water, oil, and Ethylene-Glycol (EG) for transferring the heat has been one of the great challenges on the heat transfer science. One of the ways to overcome this problem is to replace conventional fluids with some advanced fluids with higher thermal conductivities [1–7].

Due to the importance of heat exchangers in many engineering applications, the subject of potential heat transfer enhancement in these devices has received substantial attention in research and practice. In the field of heat exchanger performance, it is known that utilization of the elliptic annulus can potentially lead to better heat transfer performance due to enhanced mixing of the fluid by the elliptic annulus. However, even more improvements in heat exchanger performance are sought after in order to meet the industry requirements and demands for higher heat transfer performance. Research on the methods for heat transfer enhancement in heat exchangers has received great attention in order to cater to the growing needs of higher efficiencies in these

devices. For this purpose, in recent years, it has been shown that adding nanoparticles to the traditional heat transfer fluids (such as water, oil and ethylene glycol), can lead to improvement in their thermal conductivity. These so called 'nanofluids' can be applied in heat exchangers to enhance the heat transfer, leading to higher heat exchanger efficiency [8–24].

Heat transfer is categorized into numerous mechanisms, such as conduction, convection, and radiation. Convection is one of the chief methods of heat transfer that can be qualified in terms of being natural, forced, gravitational, granular, or thermomagnetic. Combined convection heat transfer exists when natural convection currents are the same order of magnitude as forced flow velocities [25]. The term 'mixed convection' means that the flow occurs when both natural (free) and forced convection mechanisms concurrently and significantly contribute to the heat transfer. The relative contribution of each mechanism depends on the flow regime (laminar or turbulent), magnitude of the temperature driving force for heat transfer, magnitude of Reynolds number, and orientation (vertical, horizontal, angled) [26].

Mixed convection heat transfer and fluid flow in an annulus is a significant phenomenon in engineering systems as it as, a common and essential geometry for fluid flow and heat transfer devices. It has a lot of engineering applications such as in double pipe heat exchanger, gas turbines, nuclear reactors, turbo machinery, thermal storage systems,

* Corresponding author.
  E-mail address: hussein.dash@yahoo.com (H.A. Mohammed).

Nomenclature

A	surface area,(m^2)
L	length of annulus, (m)
M	molecular weight, (mol)
Re	Reynolds number, ($Re = u_{av} D_h/v$)
g	acceleration due to gravity (m/s^2)
dp	diameter of nanofluid particles, (nm)
D_{in}	inner diameter, (m)
D_H	hydraulic diameter, (m) ; ($D_h = 4A/P$)
R_o	outer radius, (m)
Ra	Rayleigh number, ($Ra = Gr.Pr$)
T_{in}	inner cylinder temperature, (K)
K	thermal conductivity, (W/m. K)
N	Avogadro number
Al_2O_3	aluminum oxide
CuO	copper oxide
Gr	Grashoff number, ($Gr = \beta\, g\, L^3(T_i\text{-}T_o)\,/\,v^2$)
t	time, (s)
P	pressure, (Pa)
f	friction factor, (f = (2ΔPDh) /(Lρu_{av}^2))
HRR	hydraulic radius ratio
Nu	Nusselt number, ($Nu = h\, D_h/k$)
H	heat transfer coefficient, (W/m^2 K)
D_o	outer diameter, (m)
R_{in}	inner radius, (m)
Pr	Prandtl number, ($Pr = C_p\, \mu/k$)
v	inlet velocity,(m/s)
C_p	specific heat, (KJ/kg.K)
q	cylinder heat flux, (W/m^2)
ΔP	dimensionless pressure drop
SiO_2	silicon oxide
ZnO	zinc oxide
EG	ethylene glycol

Greek symbols

ρ	Density of the fluid, (kg/m^3)
μ	dynamic viscosity, (N.m/s)
υ	kinematic viscosity, (m^2/s)
β	thermal expansion coefficient, (1/K)
κ	Boltzmann constant
Φ	nanoparticles volume fraction (%)

Subscripts

bf	base fluid
nf	nanofluid
np	nanoparticle
H	hydraulic
eff	effective
Av	average
S	solid
O	outlet

aircraft fuselage insulation to underground electrical transmission cables, solar energy systems, boilers, cooling of electronic devices, compact heat exchangers, cooling core of nuclear reactors, cooling systems, gas-cooled electrical cables, thermal insulation, electrical gas insulated transmission lines ventilation and air conditioning system [27].

The heat transfer enhancement technology has been improved and widely used in heat exchanger applications. One of the widely used heat transfer enhancement technique is inserting different shaped elements with different geometries in channel flow [28–30]. Akbarinia and Behzadmehr [31] numerically investigated the fully developed laminar mixed convection of Al_2O_3–water nanofluid flowing through a horizontal curved tube. In their studies, three-dimensional elliptic governing equations were used. The effects of the buoyancy force, centrifugal force and particle concentration on the heat transfer performance were presented. The results showed that the particle concentration has no direct effect on the secondary flow, axial velocity and skin friction coefficient. However, when the buoyancy force is more important than the centrifugal force, the effect of particle concentration on the entire fluid temperature can affect the hydrodynamic parameters. Moreover, the results also indicated that the buoyancy force decreases the Nusselt number whereas the particle concentration has a positive effect on the heat transfer enhancement and on the skin friction reduction. Ben Mansour et al. [32] experimentally investigated the thermally developing laminar mixed convection flow of water and Al_2O_3 mixture inside an inclined tube with a uniform wall heat flux. They observed that a higher particle volume concentration clearly induces a decrease of the Nusselt number for the horizontal inclination. On the other hand, for the vertical one, the Nusselt number remains nearly constant with an increase of particle volume concentration from 0 to 4%. The apparent contradictory behavior observed between experimental data and analytical/numerical results regarding the heat transfer enhancement of nanofluids prompted them to raise serious concerns regarding the applicability of using the single phase and homogeneous fluid model for nanofluids under natural convection effect.

Conceptually, investigation of the heat transfer enhancement in annuluses is essential. Some researchers have been considering application of the nanofluids in annulus [33–35]. Abu-Nada [33] has studied single phase Al_2O_3–water nanofluid flow in an annulus. Different viscosity and thermal conductivity models are used to evaluate heat transfer enhancement in the annulus by his work. Bianco et al. [34] investigated the heat transfer performance of an Al_2O_3–water nanofluid flowing through a circular tube under a laminar flow regime numerically. A single-phase model and two-phase model were used to determine the heat transfer coefficient of the nanofluid. The results demonstrated that the heat transfer performance increases with increasing Reynolds number as well as particle volume concentration. Moreover, differences in the average heat transfer coefficient between the single-phase and two-phase models were observed as approximately 11%. Abu-Nada et al. [35] have studied various nanofluids consisting base water and different nanoparticles such as Cu, Ag, Al_2O_3 and TiO_2 in horizontal annulus with single phase approaches.

Many attempts in this field have been completed to formulate appropriate effective thermal conductivity and dynamic viscosity of nanofluid [36–38]. Teng et al. [39] have measured the effects of

Table 1
The thermophysical properties of different nanoparticles and different base fluids at T = 300 K.

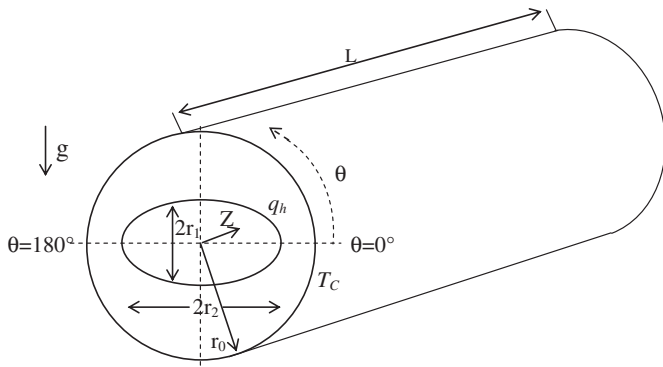| Thermophysical properties Ref.	Al_2O_3 [48]	CuO [48]	SiO_2 [49]	ZnO [49]	Glycerine [50]	Engine oil [50]	EG [50]
ρ (kg/m^3)	3970	6500	2200	5600	1259.9	884.1	1114.4
Cp (J/kg·K)	765	535.6	703	495.2	2427	1909	2415
k (W/m·K)	40	20	1.2	13	0.286	0.145	0.252
μ (Ns/m^2)	–	–	–	–	0.799	0.486	0.0157
β (1/K)	5.8×10^{-6}	4.3×10^{-6}	5.5×10^{-6}	4.31×10^{-6}	4.8×10^{-4}	7×10^{-4}	6.5×10^{-6}

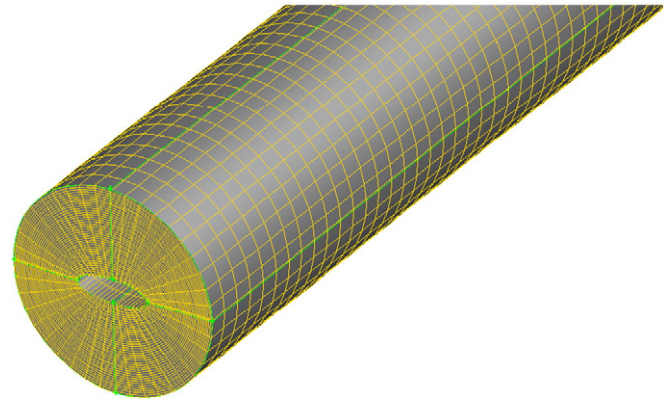Fig. 1. Schematic diagram of the computational domain of annulus.

Fig. 2. Structured non-uniform grid used for an annulus.

temperature, nanoparticles size and weight fraction on the thermal conductivity of Al$_2$O$_3$–water nanofluid. They compared their results with numerical results and proposed a good correlation for thermal conductivity, which depends on temperature, nanoparticles size and weight fraction. Recently, Das et al. [40] and Putra et al. [41] have investigated a water–Al$_2$O$_3$ mixture experimentally and found that increasing temperature increases the effective thermal conductivity remarkably while the dynamic viscosity decreases. Yu et al. [42] measured the thermal conductivity of ZnO-EG nanofluid. They establish that the enhanced value of 5.0 vol.% ZnO-EG nanofluid is 26.5%, well beyond the values given by the existing classical models for the solid liquid mixture, and it is consistent with the prediction values by the combination of the aggregation mechanism with the Maxwell and Bruggeman models. Murshed et al. [43] have done a similar experimental work, which has considered the effects of particle size, nanolayer, Brownian motion, and particle surface chemistry and interaction potential on the thermal conductivity of nanofluids, and proposed a new model for thermal conductivity.

It can be seen from the above literature review that the heat transfer enhancement of laminar mixed convection flow using nanofluids in an elliptic annulus under constant heat flux boundary condition seems not to have been investigated in the past and this has motivated the present study. In addition, most of the previous research on elliptic annulus involved conventional fluids (not nanofluids) and there is a very little work reported in the open literature that involved nanofluids in elliptic annulus. However, there is no previous research that involved the usage of nanofluid in an elliptic annulus. The current study examines 3D laminar mixed convective heat transfer in the elliptic annulus with uniform heat flux by using different types of nanofluids, different nanoparticle volume fractions, and different nanoparticle diameters, are dispersed in different base fluids (ethylene glycol, glycerine, engine oil and water). This investigation covers Reynolds number in the range of 200 to 1000 and particle diameters range from 20 to 80 nm. Different types of nanofluids (Al$_2$O$_3$, SiO$_2$, CuO and ZnO) and different volume fractions ranged from 0% to 4%. Results of interests such as Nusselt number and friction factor for laminar mixed convection heat transfer in an

elliptic annulus are reported to illustrate the effect of nanofluids on these parameters.

2. Numerical model

2.1. Physical model

The physical model of the test section mainly consists of two concentric horizontal cylinders used to form an annular space ranging from an elliptical tube placed at the center of a circular cylinder. The outer cylinder was made from aluminum of 50.8 mm outer diameter, 1 mm thickness, and 500 mm length. The inner elliptic cylinder was made of aluminum with a major radius (r$_2$) of 9 mm and a length of 500 mm that had an axis ratio (r$_1$/ r$_2$ = 1/3). Pure ethylene glycol, various nanoparticles and various base fluids are selected as the working fluid and the thermophysical properties assumed to be temperature independent. The thermo-physical properties of ethylene glycol and nanoparticle materials used for simulation are shown in Table 1. The internal wall of the annular space (elliptic tube surface) was maintained under constant heat flux (q$_h$). Whereas the external wall of the annular space (circular cylinder surface) was kept isothermally at a constant temperature (T$_c$). The schematic diagram of the annular space under consideration and coordinate system are shown in Fig. 1.

2.2. Geometry and the governing equations

The three-dimensional Navier–Stokes and energy equations were used to describe the flow and heat transfer in the annuals. Heat is transferred between the fluids through the wall which is separating them. Numerous assumptions were made on the operating conditions of the annulus: (i) the annulus operates under steady-state conditions and three-dimensional; (ii) the nanofluid is Newtonian and incompressible; (iii) fluid is in single phase and the flow is laminar; (iv) the external heat transfer effects are ignored; (v) the outer walls of the annulus are adiabatic; and (vi) constant thermophysical properties are considered for the nanofluid, except for the density variation in the buoyancy forces, determined by using the Boussinesq approximation where the approximation is applicable for sufficiently small temperature difference between the inner and outer cylinders. The numerical prediction of the conjugate heat transfer was conducted using the CFD code FLUENT 6.3.26. The CFD modeling involves numerical solutions of the conservation equations for continuity, momentum and energy.
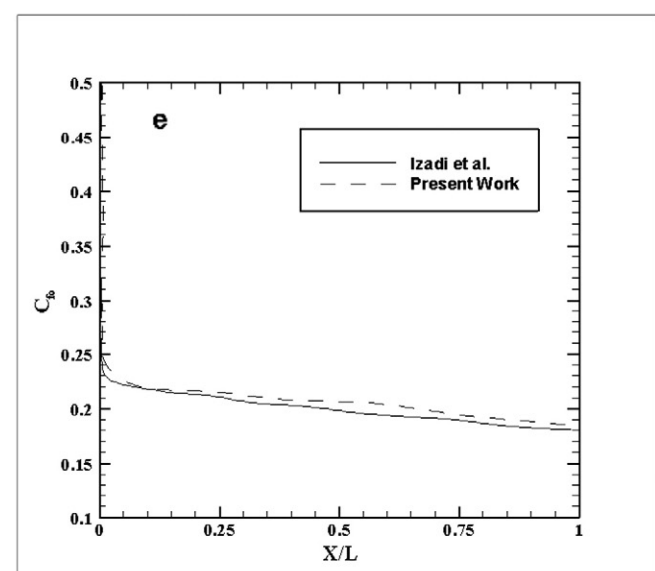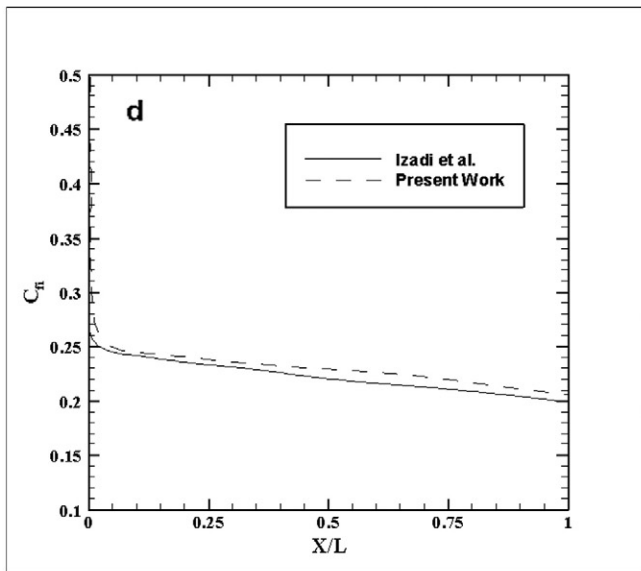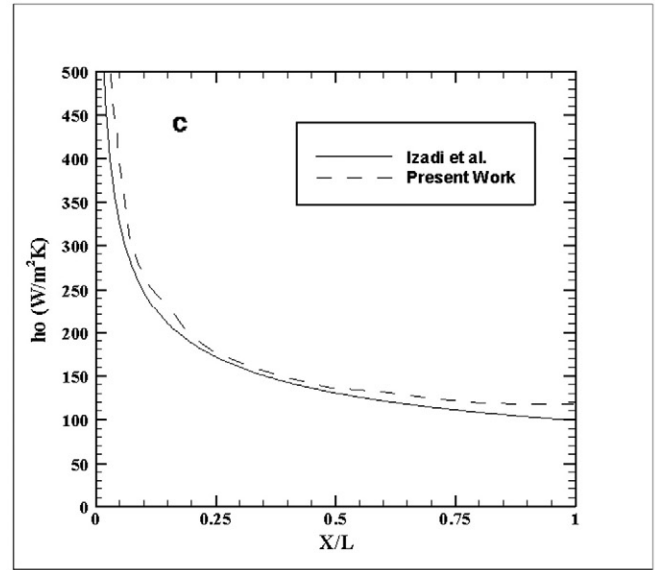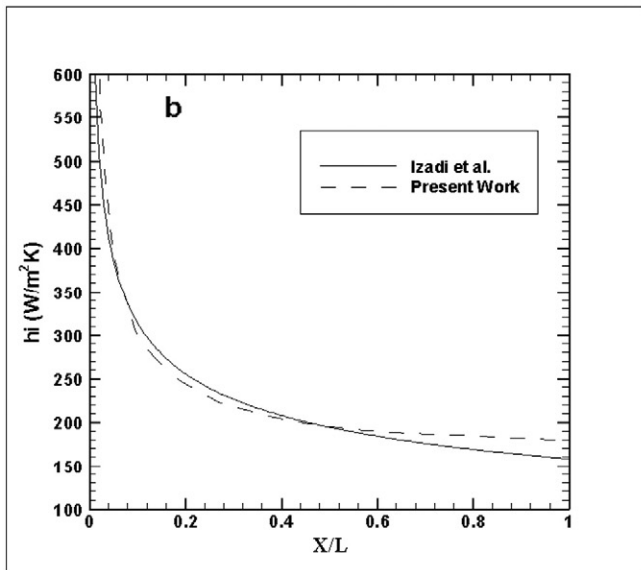
The governing equations for flow and heat transfer in the annulus are as follows [44]:

Continuity equation:

Table 2
The values of β for different particles with its boundary conditions [46,47].

Type of particles	β	Concentration	Temperature
Al$_2$O$_3$	$8.4407(100\phi)^{-1.07304}$	$1\% \leq \phi \leq 10\%$	
	298 K $\leq T \leq$ 363 K		
CuO	$9.881(100\phi)^{-0.9446}$	$1\% \leq \phi \leq 6\%$	
	298 K $\leq T \leq$ 363 K		
SiO$_2$	$1.9526(100\phi)^{-1.4594}$	$1\% \leq \phi \leq 10\%$	
	298 K $\leq T \leq$ 363 K		
ZnO	$8.4407(100\phi)^{-1.07304}$	$1\% \leq \phi \leq 7\%$	
	298 K $\leq T \leq$ 363 K		

$$\frac{\partial \rho}{\partial t} + \frac{1}{r}\frac{\partial}{\partial r}(\rho r v_r) + \frac{1}{r}\frac{\partial}{\partial \theta}(\rho v_\theta) + \frac{\partial}{\partial z}(\rho v_z) = 0 \tag{1}$$
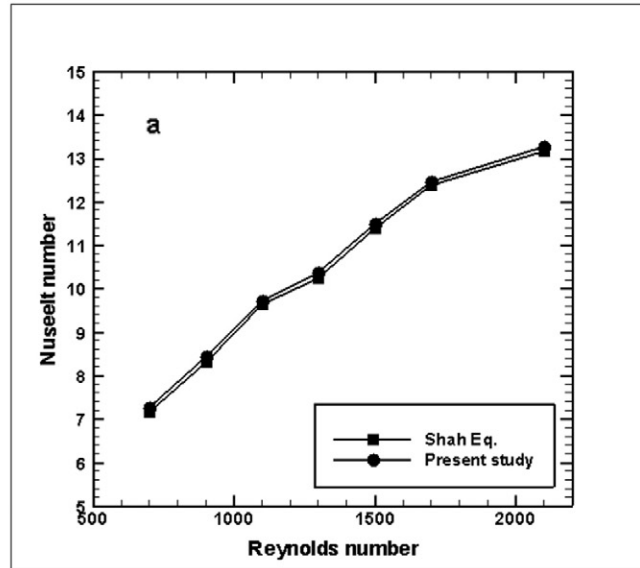
R –Momentum equation:

$$\rho\left(v_r\frac{\partial v_r}{\partial r} + \frac{v_\theta}{r}\frac{\partial v_r}{\partial\theta} - \frac{v_\theta^2}{r} + v_z\frac{\partial v_r}{\partial z} + \frac{\partial v_r}{\partial t}\right) =$$
$$\rho g_r - \frac{\partial p}{\partial r\partial} + \mu\left[\frac{\partial}{\partial r}\left(\frac{1}{r}\frac{\partial}{\partial r}(rv_r)\right) + \frac{1}{r^2}\frac{\partial^2 v_r}{\partial\theta^2} - \frac{2}{r^2}\frac{\partial v_\theta}{\partial\theta} + \frac{\partial^2 v_r}{\partial z^2}\right]$$

(2a)

θ –Momentum equation:

$$\rho\left(v_r\frac{\partial v_\theta}{\partial r} + \frac{v_\theta}{r}\frac{\partial v_\theta}{\partial\theta} + \frac{v_r v_\theta}{r} + v_z\frac{\partial v_\theta}{\partial z} + \frac{\partial v_\theta}{\partial t}\right) =$$
$$\rho g_\theta - \frac{1}{r}\frac{\partial p}{\partial\theta} + \mu\left[\frac{\partial}{\partial r}\left(\frac{1}{r}\frac{\partial}{\partial r}(rv_\theta)\right) + \frac{1}{r^2}\frac{\partial^2 v_\theta}{\partial\theta^2} + \frac{2}{r^2}\frac{\partial v_r}{\partial\theta} + \frac{\partial^2 v_\theta}{\partial z^2}\right]$$

(2b)

Z –Momentum equation:

$$\rho\left(v_r\frac{\partial v_z}{\partial r} + \frac{v_\theta}{r}\frac{\partial v_z}{\partial\theta} + v_z\frac{\partial v_z}{\partial z} + \frac{\partial v_z}{\partial t}\right) =$$
$$\rho g_z - \frac{\partial p}{\partial z} + \mu\left[\frac{1}{r}\frac{\partial}{\partial r}\left(r\frac{\partial v_z}{\partial r}\right) + \frac{1}{r^2}\frac{\partial^2 v_z}{\partial\theta^2} + \frac{\partial^2 v_z}{\partial z^2}\right]$$

(2c)

Energy equation:

$$\rho c_p\left(\frac{\partial T}{\partial t} + v_r\frac{\partial T}{\partial r} + \frac{v_\theta}{r}\frac{\partial T}{\partial\theta} + v_z\frac{\partial T}{\partial z}\right) = k\left[\frac{1}{r}\frac{\partial}{\partial r}\left(r\frac{\partial T}{\partial r}\right) + \frac{1}{r^2}\frac{\partial^2 T}{\partial\theta^2} + \frac{\partial^2 T}{\partial z^2}\right] + \mu\phi$$

(3)

These governing equations with the given boundary conditions are solved to obtain the fluid Nusselt number distribution along the annulus. These data were then used to examine the thermal field along the annulus.

The Nusselt number, the Reynolds number and the friction factor are dimensionless parameters which are calculated, respectively, as follows [6]:

$$Nu = \frac{hD_h}{k}$$

(4)

Where k and h are the thermal conductivity and average heat transfer coefficient of fluid, respectively.

The Reynolds number is defined as:

$$Re = \frac{\rho u_m D_h}{\mu}$$

(5)

Where ρ, u_m, and μ are density, mean fluid velocity over the cross-section and dynamic-viscosity of fluid, respectively. The hydraulic diameter (D_h) is defined as:

$$D_{h = \frac{4A}{P}}$$

(6)

Where A is the cross area and P is the wetted perimeter of the cross-section.

The friction factor for fully developed flow is expressed as follows:

$$f = \frac{2\Delta p\, D_h}{L\,\rho\,u_m^2}$$

(7)

2.3. Boundary conditions

At the elliptic inlet, different velocities depending on the values of Reynolds number were used, and the outlet temperature was taken as

$T_{in} = 300$ K. The constant heat flux used was 5000 W/m^2 to heat up the inside walls. At the domain outlet the flow and heat transfer are assumed to be fully developed. The boundary condition can be expressed as follow:

• At the inlet of annulus (z = 0 and $r_i \leq r \leq r_o$):

$$u_r = u_\theta = u_z = 0, \text{and } T = T_i$$

(8)

• At the fluid wall interface: (r = r_i and $0 \leq z \leq L$)

$$u_r = u_\theta = u_z = 0,$$
$$\text{and } q_{w,i} = -k_{eff}\frac{\partial T}{\partial r}\bigg|r = ri$$

(9)

• At the outlet of annulus (z = L and $r_i \leq r \leq r_o$): p = p$_0$ and an overall

mass balance correction is applied.

2.4. Thermophysical properties of nanofluids

The thermophysical properties of pure ethylene glycol (EG), various nanoparticles and various base fluids which are density, heat capacity, effective dynamic viscosity, effective thermal conductivity and thermal expansion coefficient are given in Table 1. These properties are calculated using the following equations:

Density [45]:

$$\rho_{eff} = (1-\phi)\rho_{bf} + \phi\rho_{np}$$

(9)

Heat capacity [46]:

$$(Cp)_{eff} = \frac{(1-\phi)(\rho Cp)_{bf} + \phi(\rho Cp)_{np}}{(1-\phi)\rho_{bf} + \phi\rho_{np}}$$

(10)

Effective thermal conductivity [45]:

$$k_{eff} = k_{static} + k_{Brownian}$$

(11)

Static thermal conductivity [45]:

$$k_{static} = k_{bf}\left[\frac{(k_{np} + 2k_{bf}) - 2\phi(k_{bf} + 2k_{np})}{(k_{np} + 2k_{bf}) + \phi(k_{bf} + 2k_{np})}\right]$$

(12)

Brownian thermal conductivity [45]:

$$k_{Brownian} = 5\times 10^4\beta\phi\rho_{bf}C_{pbf}\sqrt{\frac{kT}{2\rho_{np}R_{np}}}f(T,\phi)$$

(13)

Modeling function, $f(T,\phi)$ [46]:

$$f(T,\phi) = (0.028217\phi + 0.003917)\frac{T}{T_o} + (0.030669\phi - 0.00391123)$$

(14)

Where K is the Boltzman constant ($\kappa = 1.3807\times 10^{-23}$ J/K), T is the fluid temperature and T_0 is the reference temperature. The term of $f(T,\varnothing)$ is a function of temperature and particle volume fraction. The

Fig. 3. Comparison of the heat transfer coefficient and friction factor at (b) & (d) inner wall and (c) & (e) outer wall respectively with published numerical results carried out by Izadi et al. [1] at $Re = 900$, Ø = 0.03, qi/qo = 1, dp = 25 mm.
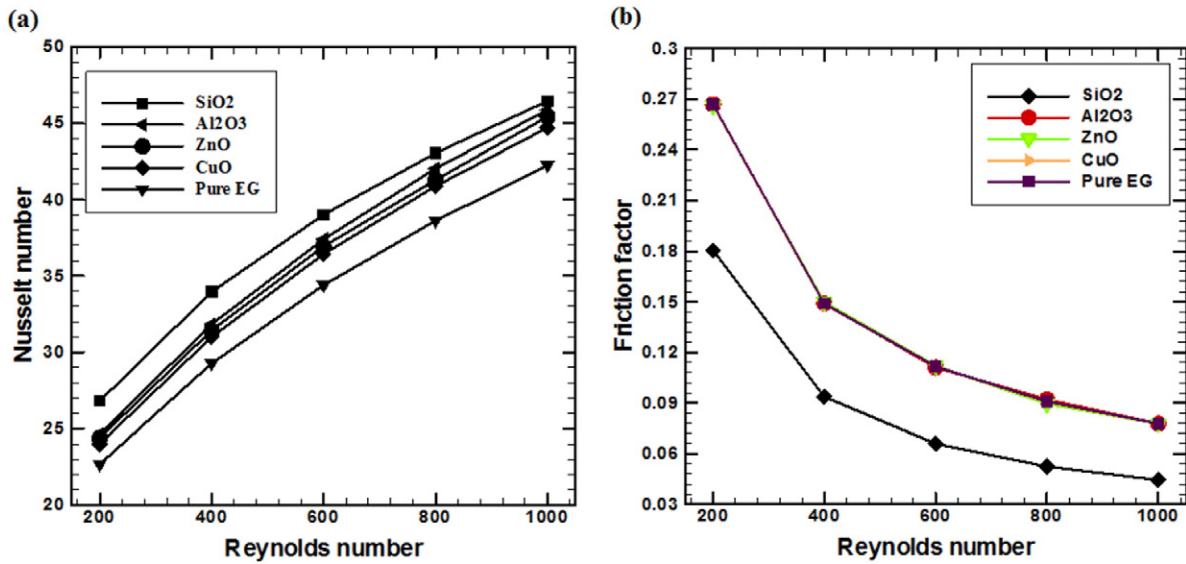
Fig. 4. The effect of different nanofluids types at different Reynolds numbers, (a) Nusselt number, and (b) Friction factor.

correlation of β is a function of the liquid volume that travels with a particle material expressed in Table 2 as it is given by Vijjha [47].

Dynamic viscosity [48]:

$$\frac{\mu_{eff}}{\mu_{bf}} = \frac{1}{1 - 34.8\left(\frac{d_{np}}{d_{bf}}\right)^{-0.3}\phi^{1.03}} \qquad (15)$$

Where $d_{bf} = [6M/N\pi\rho_{bf}]^{1/3}$ μ_{eff} and μ_{bf} are the effective dynamic viscosity of nanofluid and dynamic viscosity of the base fluid respectively, d_{np} is the nanoparticle diameter, d_{bf} is the base fluid equivalent diameter and ϕ is the nanoparticle volume fraction. M is the molecular weight of the base fluid, N is the Avogadro number $= 6.022 \times 1023\,mol^{-1}$ and ρ_{fo} is the mass density of the base fluid calculated at temperature To = 293 K.

2.5. Numerical parameters and procedures

The numerical computations were carried out by solving the governing conservation along with the boundary conditions using the finite volume method (FVM) with the aid of commercial software (FLUENT©). SIMPLE algorithm is used to solve the flow field inside an annulus. The diffusion term in the momentum and energy equations is approximated by first-order central difference which gives a stable solution. In addition, a first-order upwind differencing scheme is adopted for the convective terms [51]. An unstructured non uniform grid distribution has been used to discretize the computational domain as shown in Fig. 2. The numerical model was developed in the physical domain, and dimensionless parameters were calculated from the computed velocity and temperature distributions. The residual sum for each of the conserved variables is computed and stored at the end of each the iteration. The convergence criterion required that the maximum relative mass residual based on the inlet mass be smaller than 1×10^{-6}.

2.6. Grid testing and code validation

The computational domain resulted from the subtraction of the elliptical cylinder section from the circular cylinder section. The grid is made up of triangular elements to improve the quality of the numerical prediction near the curved surfaces as shown in Fig. 2. Four different
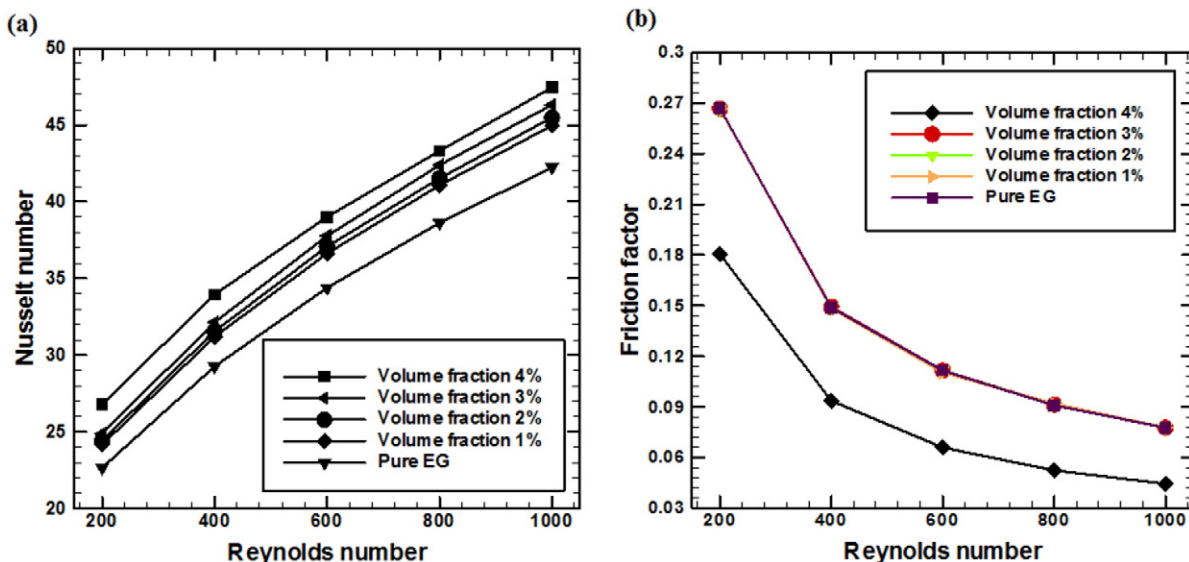

Fig. 5. The effect of different volume fractions of nanoparticles at different Reynolds numbers, (a) Nusselt number, and (b) Friction factor.
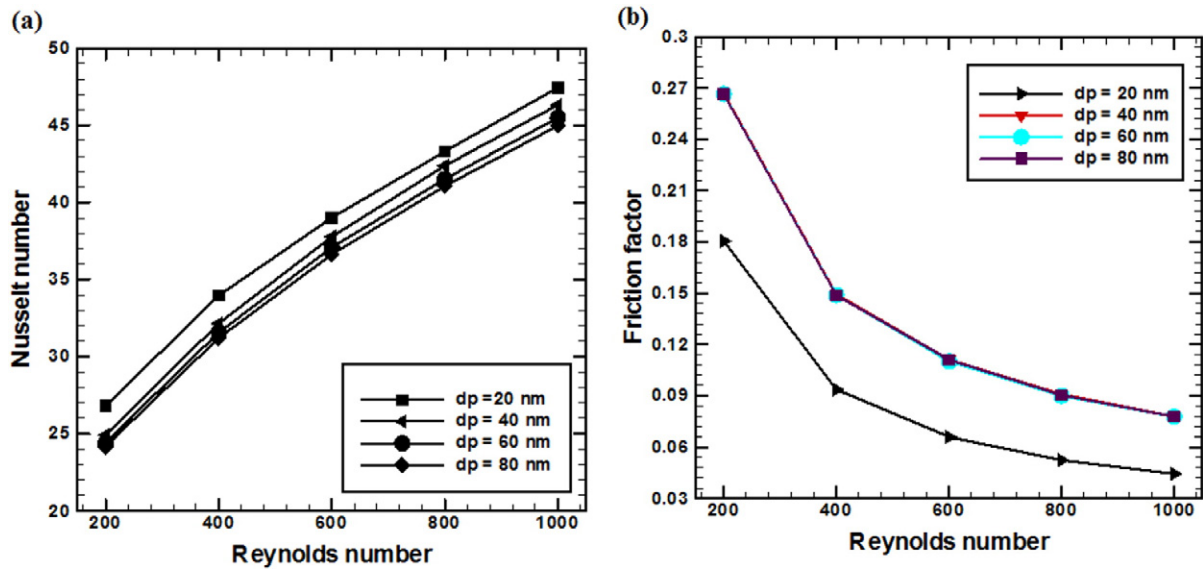
Fig. 6. The effect of different nanoparticles diameters at different Reynolds numbers, (a) Nusselt number, and (b) Friction factor.

sets of the grid sizes were imposed to the geometry and simulated by calculating the Nusselt number at $Re = 1000$. The four grids sizes are $40 \times 10 \times 100$, $20 \times 10 \times 200$, $50 \times 10 \times 200$ and $40 \times 30 \times 100$ show no much difference in the values of Nusselt number. Thus, the grid size of $40 \times 10 \times 100$ is selected in this study as it is found to provide a more stable grid independent solution. The code validation was done based on the geometry and boundary conditions which were used by Izadi et al. [1]. They studied the thermal characteristics of laminar and turbulent convection heat transfer in an elliptic annulus with constant heat flux boundary condition. In this case, the results of the Nusselt number variation were compared with the predictions of the following well-known Shah equation for laminar flows under the constant heat flux boundary condition [1] as shown in Fig. 3a. To validate the accuracy of the numerical solutions, the Nusselt number (Nu) and the friction factor (f) of the elliptic annular is compared with the theoretical data. It is clearly seen that the deviation between the numerical results and the theoretical data is 5% by Izadi et al. [1] as shown in Fig. 3b–e. Therefore, the present numerical predictions have reasonable accuracy.

3. Results and discussion

In this work, laminar heat transfer and fluid flow for different types of nanofluids in a three-dimensional through an elliptic annulus is examined. Five values of Reynolds number were used in the range of $200 \leq Re \leq 1000$ and four nanoparticles volume friction in the range of $0 \leq \phi \leq 0.04$. The ethylene glycol was considered as a base fluid. Four different types of nanoparticles are studied which are, Al_2O_3, CuO, SiO_2 and ZnO. The nanoparticles diameter was in the range of $20\ nm \leq dp \leq 80\ nm$. The effects of particle type, volume fraction, particle diameter, Reynolds number and different base fluids on the Nusselt number and friction factor are presented and interpreted in this section.

3.1. The effects of nanofluids on the thermal field

The effects of different nanoparticle types on the thermal fields are presented via the Nusselt number. The base fluid considered is pure EG and the nanoparticle diameter and concentrations are set to 20 nm and 4% respectively. The nanoparticle type affects the nanofluid
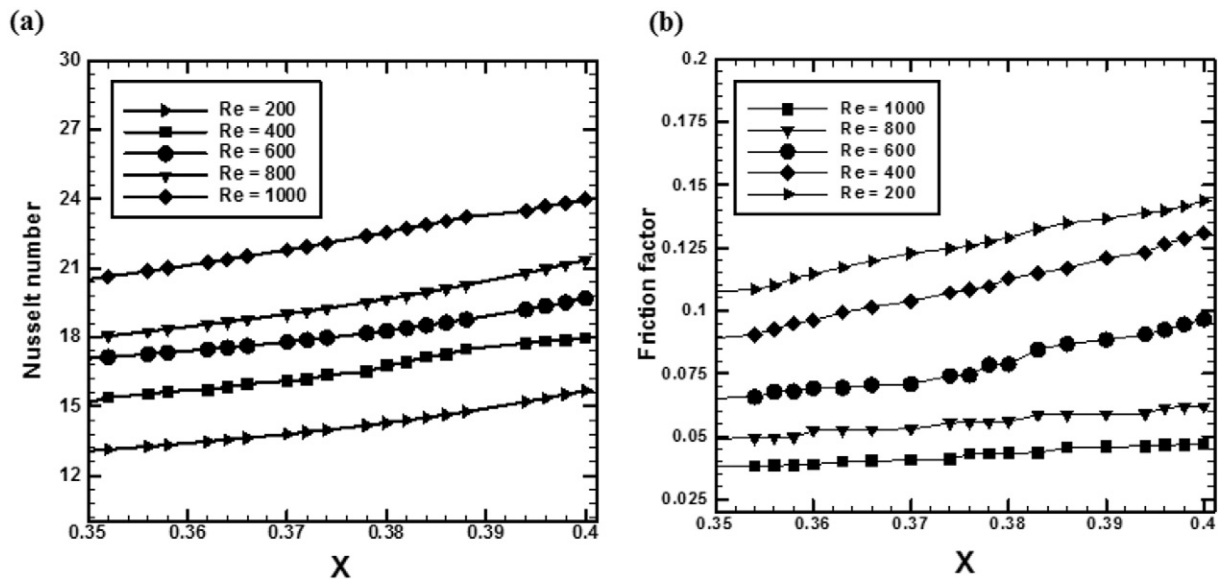

Fig. 7. The effect of different Reynolds numbers at x-position, (a) Nusselt number, and (b) Friction factor.
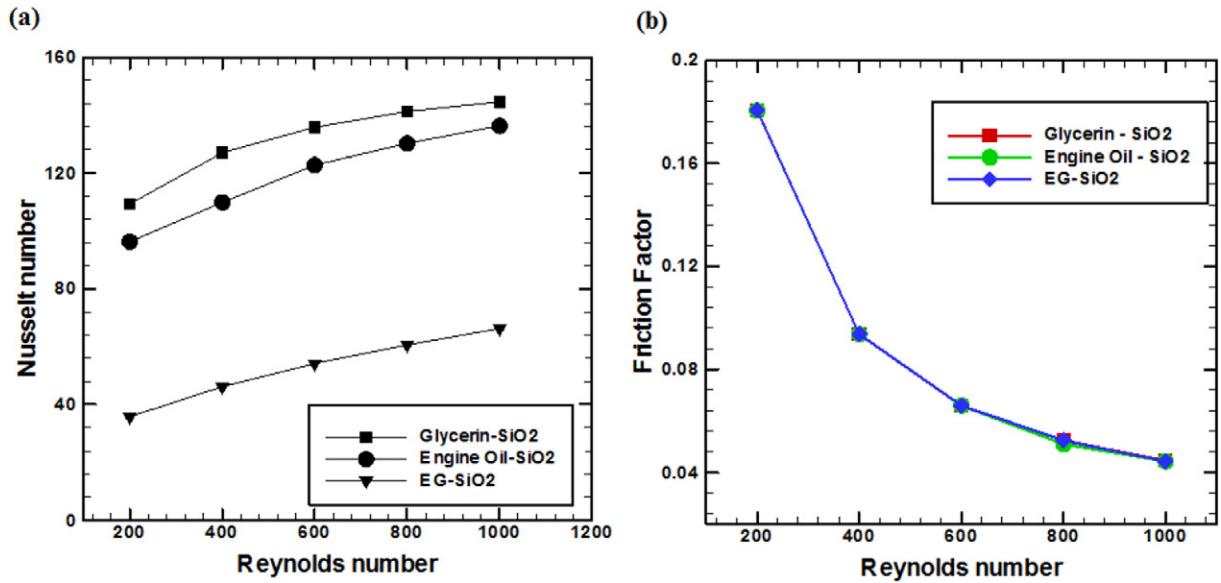
Fig. 8. The effect of different base fluids at different Reynolds numbers, (a) Nusselt number, and (b) Friction factor.

properties which in turn affect the heat transfer performance. The Nusselt number for different values of Reynolds number and different nanofluids are shown in Fig. 4a. It is observed that SiO_2 nanofluid has the highest surface Nusselt number and velocity, followed by Al_2O_3, ZnO, and CuO respectively. This is because SiO_2 has the lowest thermal conductivity than other nanofluids, but higher than EG and has the highest average velocity among other fluids due to its lowest density compared with the others. The Nusselt number increases significantly as Reynolds number increases for the four nanofluids types. It is less dense and this property enables the particle to move rapidly in the tube and it characterizes the main reason to give high heat transfer co-efficient. In universal, the value of Nusselt number is inversely proportional to the value of thermal conductivity of that particular fluid.

The effect of different nanofluids on the friction factor with a Reynolds number is displayed in Fig. 4b where the particle volume fraction and nanoparticle diameter are kept constant at 4% and 20 nm respectively. It is clearly seen that the friction factor decreases when Reynolds

number increases for all types of nanofluids. It is found that SiO_2 nanofluid has the highest friction factor, followed by Al_2O_3, ZnO, and CuO nanofluids and finally pure EG. The suspension of nanoparticles in the base fluid causes a slight increase in the friction factor.

3.2. The effect of different nanoparticles volume fractions

In this study, the effect of nanoparticle volume fraction in the range of 0%–4% with different values of the Reynolds number and diameter of particle $dp = 20$ nm is investigated. As shown clearly in Fig. 5a, increasing nanoparticle volume fraction enhances the Nusselt number. The results showed that the Nusselt number is not very sensitive to the volume fraction of nanoparticles at lower Reynolds number and in all cases with increasing the Reynolds number, the Nusselt number increases. This is because as the volume fraction increases, irregular and random movements of the particles increases the energy exchange rates in the fluid with penalty on the wall shear stress and consequently
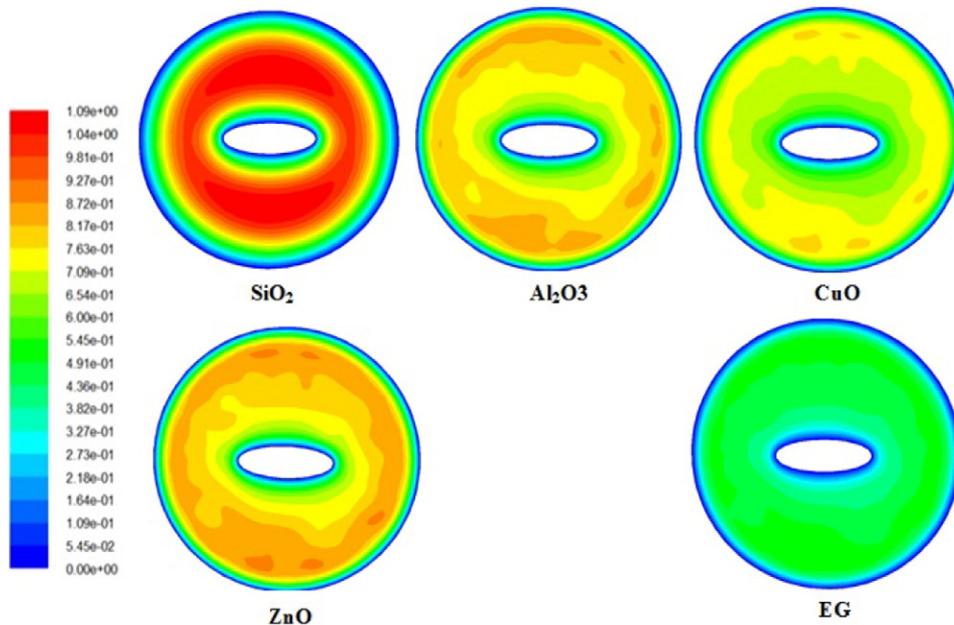

Fig. 9. The contours of velocity profile of different nanoparticle types. (a) SiO_2 (b) Al_2O_3 (c) CuO (d) ZnO and (e) EG for $Re = 1000$, $\phi = 0.04$, $dp = 20$ nm in the annulus tube.
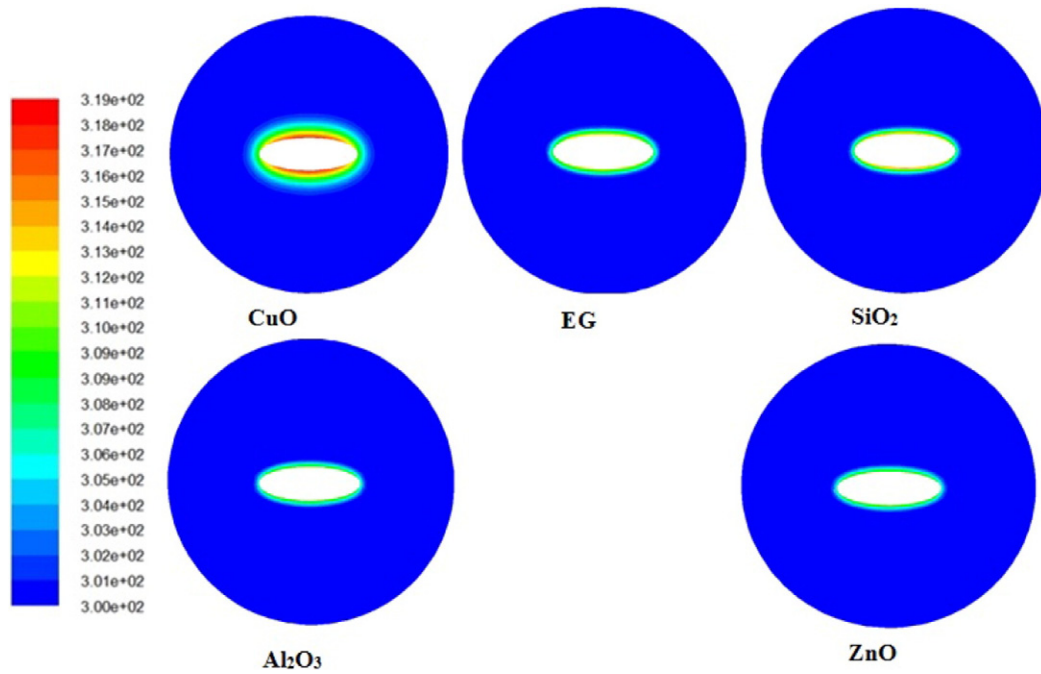
Fig. 10. The contours of temperature profile of different nanoparticle types. (a) CuO (b) ZnO (c) Al_2O_3 (d) SiO_2 and (e) EG for $Re = 1000$, $\phi = 0.04$, $dp = 20$ nm in the annulus tube.

enhance the thermal dispersion of the flow. It is also found that the surface Nusselt number increases with the increase of Reynolds number. As shown in Fig. 5b the friction factor decreases with the increase of Reynolds number for different volume fractions of nanoparticles. In general, the increase of nanoparticles volume fraction results in an increase of fluid viscosity which diminishes the fluid movement.

3.3. The effect of different nanoparticles diameters

This study used SiO_2-EG as a working fluid with fixed other parameters such as volume fraction 4% except that Reynolds number was in the range of 200–1000. The range of nanoparticle diameter is 20–80 nm. As illustrated in Fig. 6a, the results revealed that the nanofluid with smaller particle diameter has the higher Nusselt number. The effect of particle size may be attributed mainly to two reasons which are the high specific surface area of the nanoparticles and the Brownian motion. As the particle size reduces, the surface area per unit volume increases, the heat transfer is being dependent on the surface area, and thus the effectiveness of nanoparticles in transferring heat to the base liquid increases. However, reducing the particle size means increasing the Brownian motion velocity, which again adds up to the contribution by the nanoparticles to the total heat transfer by continuously creating additional paths for the heat flow in the fluid. As presented in this figure the nanofluid with 20 nm nanoparticle diameter has the highest Nusselt number, whereas, the nanoparticle with a diameter of 80 nm has the lowest Nusselt number.

The effect of different nanoparticle diameters of SiO_2 nanofluid on the friction factor with different Reynolds numbers is presented in Fig. 6b. It is noted that there is a slight change in the friction factor when nanoparticle diameters of SiO_2 nanofluid are varied.

3.4. The effect of different Reynolds numbers

Different values of Reynolds number in the range of $200 < Re < 1000$ were used in this study that produced variation output accordingly. From Fig. 7a, it can be observed that as the Reynolds number increases the average Nusselt number also increases. From Fig. 7a, it can clearly be seen that the Reynolds number increases the convective current becomes more and more strong and maximum value of isotherms

reduces. The difference of Nusselt number with x- position in elliptic annulus at variation Reynolds number is presented in Fig. 7a. The Reynolds number $Re = 1000$ provided the highest heat transfer enhancement over other Reynolds numbers. This is because of a strong mixing of the fluid induced form laminar flow and appearance of revenue flow between the adjacent elliptic annulus. As shown in Fig. 7a the $Re = 1000$ has the best heat transfer more than $Re = 800$, 600, 400, 200 respectively.

Fig. 7b shows the variation of friction factor with x-position at different Reynolds numbers. It can be seen that the friction factor is high at lower Reynolds number and then it tends to decrease when the Reynolds number increases.

3.5. The effect of different base fluids

The effect of different types of base fluids on the Nusselt number versus the Reynolds number is presented in Fig. 8a. It can clearly be seen that SiO_2-glycerine has the highest value of Nusselt number while SiO_2-EG has the lowest value of Nusselt number. This is because glycerine has the highest dynamic viscosity in nature compared to other base fluids and SiO_2 particles are mixed properly in glycerine which contributes to increase the thermal transport capacity of the mixture which in turn increases the Nusselt number. As shown in Fig. 8b the friction factor decreases with increasing in the Reynolds number for the different base fluids.

3.6. The effect velocity field of different types of nanoparticles

It is pointed out that increasing the radial and longitudinal velocity has a significant effect on increasing the annulus tube heat transfer rate. In order to explain the effect of nanofluid velocity on heat transfer rate, the CFD predicted the velocity magnitudes relating to the type of nanofluid and compared for $Re = 1000$ as shown in Fig. 9. It can be clearly seen that SiO_2 being the nanofluid with the lowest density shows the highest amount of pressure drop due to higher velocity followed by CuO, Al_2O_3, ZnO, and water. This can be the reason of more heat transfer rate obtained.

3.7. The effect temperature profile of different types of nanoparticles

For $Re = 1000$, $\phi = 0.04$, $dp = 20$ nm to different nanoparticle types of the heat transfer patterns in annuals zone via Temperature map contour are demonstrated in Fig. 10. In this study, the lower temperature surface corresponds to the higher convective heat transfer. The results reveal that the maximum heat transfer rate is found around elliptical inner pipe and diminishes along the radial direction. However, the higher convective heat transfer (lower temperature surface) is obtained from usage of CuO nanofluid. This means that the random movements of the CuO nanoparticles enhance the thermal dispersion than other nanoparticles. It can be clearly seen that this case is corresponding with another study.

4. Conclusions

In this paper, numerical investigations for three-dimensional laminar mixed convective flow and heat transfer using various types of nanofluids in an elliptic annulus with uniform heat flux are carried out. The heat transfer enhancement resulting from various parameters such as types of nanofluids, nanoparticle volume fraction, nanoparticle diameter, Reynolds number and base fluid type were studied. The governing equations were solved using the finite volume method with certain assumptions and appropriate boundary conditions. The results were predicted and compared based on their Nusselt number and friction factor can be made from the current study through the numerical simulation that gives the highest Nusselt number. The results show that the Nusselt number is remarkably increased by using nanofluids. It is observed that the increase of Reynolds number and nanoparticle volume fraction leads to increase in the Nusselt number. The results revealed that the increase in the nanoparticles diameter leads to decrease in the Nusselt number. The nanofluid of SiO_2 has the highest Nusselt number and friction factor values, followed by Al_2O_3, ZnO, and CuO and finally pure EG has the lowest Nusselt number. It is found that SiO_2–EG gave the best heat transfer performance compared to other nanofluids through the elliptic annulus were by using SiO_2 as the working fluid with percentage of concentration of 4%, diameter of particle (dp) of 20 nm, using Reynolds number of 1000. Results reveal that glycerine-SiO_2 gives the highest Nusselt number and friction factor followed by engine oil–SiO_2 while EG–SiO_2 gives the lowest Nusselt number.

References

[1] M. Izadi, A. Behzadmehr, D. Jalali-Vahida, Numerical study of developing laminar forced convection of a nanofluid in an annulus, Int. J. Therm. Sci. 48 (2009) 2119–2129.
[2] C.S. Nor Azwadi, O.A. Alawi, Computational investigations on heat transfer enhancement using nanorefrigerants, J. Adv. Res. Des. 1 (2014) 35–41.
[3] Y.K. Lee, The use of nanofluids in domestic water heat exchanger, J. Adv. Res. Appl. Mech. 3 (2014) 9–24.
[4] S. Zainal, C. Tan, C. Sian, T. Siang, ANSYS simulation for Ag/HEG hybrid nanofluid in turbulent circular pipe, J. Adv. Res. Appl. Mech. 23 (2016) 20–35.
[5] A. Vatani, H. Mohammed, Turbulent nanofluid flow over periodic rib-grooved channels, Eng. Appl. Comput. Fluid Mech. 7 (2013) 369–381.
[6] H. Mohammed, A.K. Abbas, J. Sheriff, Influence of geometrical parameters and forced convective heat transfer in transversely corrugated circular tubes, Int. Commun. Heat Mass Transfer 44 (2013) 116–126.
[7] H. Mohammed, A.M. Abed, M. Wahid, The effects of geometrical parameters of a corrugated channel with in out-of-phase arrangement, Int. Commun. Heat Mass Transfer 40 (2013) 47–57.
[8] G. Ny, N. Barom, S. Noraziman, S. Yeow, Numerical study on turbulent-forced convective heat transfer of Ag/Heg water nanofluid in pipe, J. Adv. Res. Mater. Sci. 22 (2016) 11–27.
[9] S. Abubakar, C.S. Nor Azwadi, A. Ahmad, The use of Fe3O4-H2O4 nanofluid for heat transfer enhancement in rectangular microchannel heatsink, J. Adv. Res. Mater. Sci. 23 (2016) 15–24.
[10] N.M. Noh, A. Fazeli, C.S. Nor Azwadi, Numerical simulation of nanofluids for cooling efficiency in microchannel heat sink, J. Adv. Res. Fluid Mech. Therm. Sci. 4 (2014) 13–23.
[11] H. Mohammed, H.A. Hasan, M. Wahid, Heat transfer enhancement of nanofluids in a double pipe heat exchanger with louvered strip inserts, Int. Commun. Heat Mass Transfer 40 (2013) 36–46.
[12] B. Elhajjar, G. Bachir, A. Mojtabi, C. Fakih, M.C. Charrier-Mojtabi, Modeling of Rayleigh–Bénard natural convection heat transfer in nanofluids, C.R. Mec. 338 (2010) 350–354.
[13] S.B. Abubakar, C.S. Nor Azwadi, Numerical prediction of laminar nanofluid flow in rectangular microchannel heat sink, J. Adv. Res. Fluid Mech. Therm. Sci. 7 (2015) 29–38.
[14] A. Afifah, S. Syahrullail, C.S. Nor Azwadi, Natural convection of alumina-distilled water nanofluid in cylindrical enclosure: an experimental study, J. Adv. Res. Fluid Mech. Therm. Sci. 15 (2015) 1–10.
[15] H. Mohammed, A. Al-Shamani, J. Sheriff, Thermal and hydraulic characteristics of turbulent nanofluids flow in a rib–groove channel, Int. Commun. Heat Mass Transfer 39 (2012) 1584–1594.
[16] S. Shervin, C.S. Nor Azwadi, Effect of viscous and thermal forcings on dynamical features of swimming of microorganisms in nanofluids, J. Adv. Res. Fluid Mech. Therm. Sci. 17 (2016) 18–27.
[17] C.S. Nor Azwadi, I. Adamu, Turbulent force convective heat transfer of hybrid nano fluid in a circular channel with constant heat flux, J. Adv. Res. Fluid Mech. Therm. Sci. 19 (2016) 1–9.
[18] K. Narrein, H. Mohammed, Influence of nanofluids and rotation on helically coiled tube heat exchanger performance, Thermochim. Acta 564 (2013) 13–23.
[19] M. Jamil, C.S. Nor Azwadi, M.M. Yazid, Thermal performance of thermosyphon evacuated tube solar collector using TiO2/water nanofluid, J. Adv. Res. Fluid Mech. Therm. Sci. 20 (2016) 12–29.
[20] E.R.R. Tummala, E.J. Rymaszewski, Microelectronics Packaging Handbook, Cambridge Univ Press, 1997.
[21] N.C. Sidik, A. Safdari, Modelling of convective heat transfer of nanofluid in inversed L-shaped cavities, J. Adv. Res. Fluid Mech. Therm. Sci. 21 (2016) 1–16.
[22] O.A. Alawi, C.S. Nor Azwadi, S. Kazi, M.K. Abdolbaqi, Comparative study on heat transfer enhancement and nanofluids flow over backward and forward facing steps, J. Adv. Res. Fluid Mech. Therm. Sci. 23 (2016) 25–49.
[23] C. Sinz, H. Woei, M. Khalis, S.A. Abbas, Numerical study on turbulent force convective heat transfer of hybrid nanofluid, Ag/HEG in a circular channel with constant heat flux, J. Adv. Res. Fluid Mech. Therm. Sci. 24 (2016) 1–11.
[24] M. Parsazadeh, H. Mohammed, F. Fathinia, Influence of nanofluid on turbulent forced convective flow in a channel with detached rib-arrays, Int. Commun. Heat Mass Transfer 46 (2013) 97–105.
[25] H. Mohammed, O.A. Alawi, C.S. Nor Azwadi, Mixed convective nanofluids flow in a channel having forward-facing step with baffle, J. Adv. Res. Appl. Mech. 24 (2016) 1–21.
[26] H.A. Mohammed, Laminar mixed convection heat transfer in a vertical circular tube under buoyancy-assisted and opposed flows, Energy Convers. Manag. 49 (2008) 2006–2015.
[27] N. Sambamurthy, A. Shaija, G. Narasimham, M.K. Murthy, Laminar conjugate natural convection in horizontal annuli, Int. J. Heat Fluid Flow 29 (2008) 1347–1359.
[28] A.-R. Khaled, Heat transfer enhancement in hairy fin systems, Appl. Therm. Eng. 27 (2007) 250–257.
[29] D. Jehad, G. Hashim, Numerical prediction of forced convective heat transfer and friction factor of turbulent nanofluid flow through straight channels, J. Adv. Res. Fluid Mech. Therm. Sci. 8 (2015) 1–10.
[30] M.R. Abdulwahab, A numerical investigation of turbulent magnetic nanofluid flow inside square straight channel, J. Adv. Res. Fluid Mech. Therm. Sci. 1 (2014) 44–52.
[31] A. Akbarinia, A. Behzadmehr, Numerical study of laminar mixed convection of a nanofluid in horizontal curved tubes, Appl. Therm. Eng. 27 (2007) 1327–1337.
[32] R.B. Mansour, N. Galanis, C. Nguyen, Experimental study of mixed convection with water–Al 2 O 3 nanofluid in inclined tube with uniform wall heat flux, Int. J. Therm. Sci. 50 (2011) 403–410.
[33] E. Abu-Nada, Effects of variable viscosity and thermal conductivity of Al 2 O 3–water nanofluid on heat transfer enhancement in natural convection, Int. J. Heat Fluid Flow 30 (2009) 679–690.
[34] V. Bianco, F. Chiacchio, O. Manca, S. Nardini, Numerical investigation of nanofluids forced convection in circular tubes, Appl. Therm. Eng. 29 (2009) 3632–3642.
[35] E. Abu-Nada, Z. Masoud, A. Hijazi, Natural convection heat transfer enhancement in horizontal concentric annuli using nanofluids, Int. Commun. Heat Mass Transfer 35 (2008) 657–665.
[36] M. Khattak, A. Mukhtar, S.K. Afaq, Application of nano-fluids as coolant in heat exchangers: a review, J Adv. Rev. Sci. Res. 22 (2016) 1–11.
[37] C.S. Nor Azwadi, I. Adamu, M. Jamil, Preparation methods and thermal performance of hybrid nanofluids, J. Adv. Rev. Sci. Res. 24 (2016) 13–23.
[38] C. Nguyen, F. Desgranges, N. Galanis, G. Roy, T. Maré, S. Boucher, et al., Viscosity data for Al 2 O 3–water nanofluid—hysteresis: is heat transfer enhancement using nanofluids reliable? Int. J. Therm. Sci. 47 (2008) 103–111.
[39] T.-P. Teng, Y.-H. Hung, T.-C. Teng, H.-E. Mo, H.-G. Hsu, The effect of alumina/water nanofluid particle size on thermal conductivity, Appl. Therm. Eng. 30 (2010) 2213–2218.
[40] S.K. Das, N. Putra, P. Thiesen, W. Roetzel, Temperature dependence of thermal conductivity enhancement for nanofluids, J. Heat Transf. 125 (2003) 567–574.
[41] N. Putra, W. Roetzel, S.K. Das, Natural convection of nano-fluids, Heat Mass Transf. 39 (2003) 775–784.
[42] W. Yu, H. Xie, L. Chen, Y. Li, Investigation of thermal conductivity and viscosity of ethylene glycol based ZnO nanofluid, Thermochim. Acta 491 (2009) 92–96.
[43] S. Murshed, K. Leong, C. Yang, A combined model for the effective thermal conductivity of nanofluids, Appl. Therm. Eng. 29 (2009) 2477–2483.
[44] T. Adachi, S. Imai, Three-dimensional linear stability of natural convection in horizontal concentric annuli, Int. J. Heat Mass Transf. 50 (2007) 1388–1396.
[45] B. Ghasemi, S. Aminossadati, Brownian motion of nanoparticles in a triangular enclosure with natural convection, Int. J. Therm. Sci. 49 (2010) 931–940.
[46] R.S. Vajjha, D.K. Das, D.P. Kulkarni, Development of new correlations for convective heat transfer and friction factor in turbulent regime for nanofluids, Int. J. Heat Mass Transf. 53 (2010) 4607–4618.

[47] R.S. Vajjha, D.K. Das, Experimental determination of thermal conductivity of three nanofluids and development of new correlations, Int. J. Heat Mass Transf. 52 (2009) 4675–4682.

[48] M. Corcione, Heat transfer features of buoyancy-driven nanofluids inside rectangular enclosures differentially heated at the sidewalls, Int. J. Therm. Sci. 49 (2010) 1536–1546.

[49] J.H. Lienhard, A Heat Transfer Textbook, Courier Corporation, 2013.

[50] F.P. Incropera, P. Dewitt David, T.L. Bergman, A.S. Lavine, Fundamentals of Heat and Mass Transfer, sixth ed. John Wiley and Sons, 2006 (ISBN).

[51] S. Patankar, Numerical Heat Transfer and Fluid Flow, Hemisphere, New York, 1980 (There is no corresponding record for this reference. 1980).